Chapter 3

3D Printable, injectable Amyloid-based composite Hydrogel of Bovine Serum Albumin-Aloe Vera for Rapid Diabetic Wound Healing

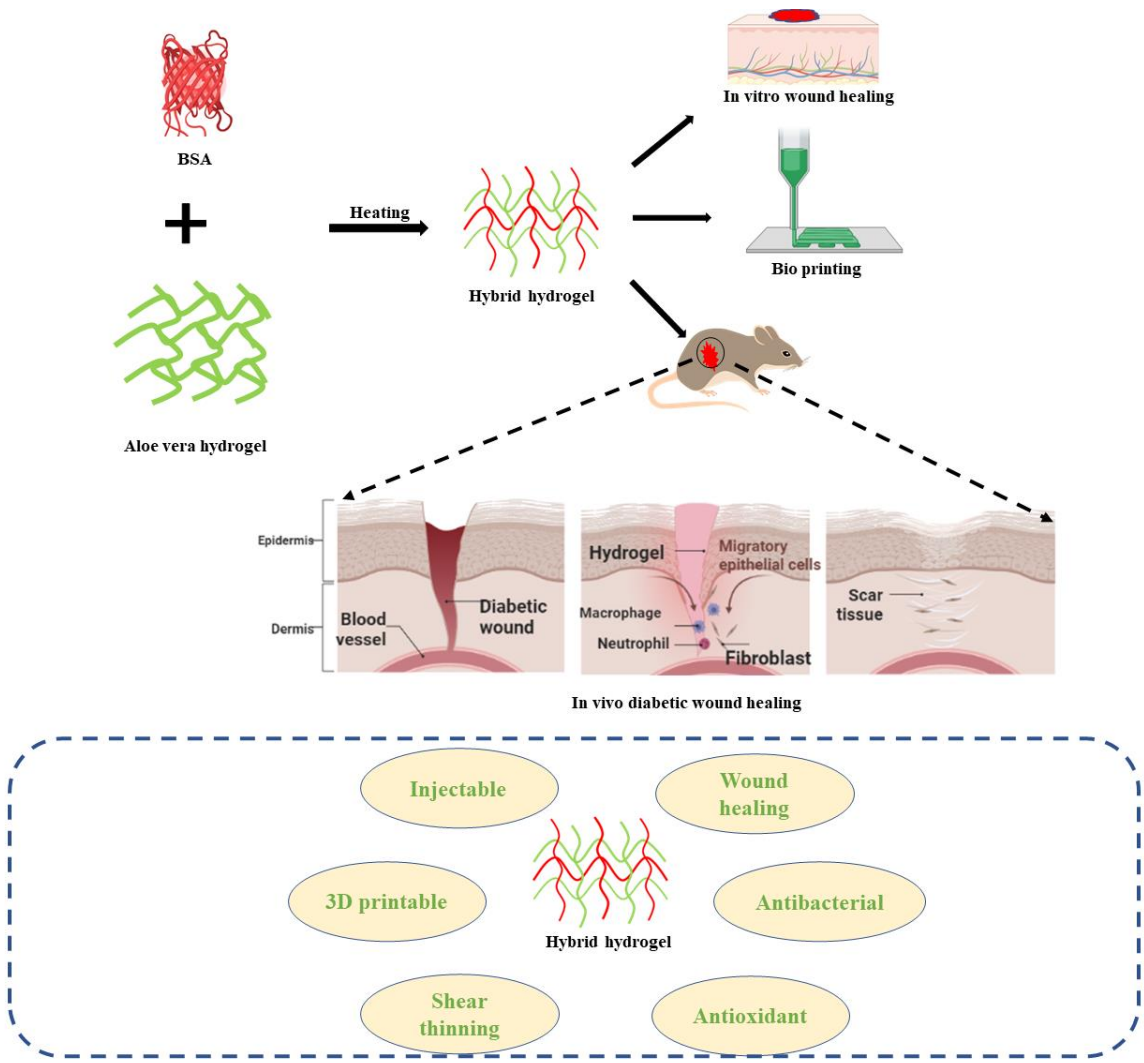

Schematic 1 for the synthesis of composite hydrogel of BSA and AV for chronic wound healing.

3.1 INTRODUCTION

Having achieved significant accomplishments in academic research and commercialization over the past decade, hydrogels have emerged as a captivating wonder of modern materials science. Researchers and engineers alike are utterly enthralled by their unique and diverse characteristics, as well as their vast potential for a multitude of exciting applications. Composed of a three-dimensional network of water-soluble polymers, hydrogels can absorb and retain large amounts of water. This class of biomaterials possesses exceptional and fascinating properties such as a highly porous structure, high water content, controlled biodegradability, tuneable mechanical and rheological properties, and low immunogenicity. In the past decade, they have garnered significant interest owing to their excellent properties for use in a wide range of biomedical applications including tissue engineering[35],[36], drug delivery[37],[38], wound dressing[39],[40], artificial organs[41],[42], regenerative medicine[43],[44], and wearable sensors.[45],[46] In recent years, naturally occurring hydrogels, made from biomolecules or derived from medicinal plants, have received considerable interest for biomedical purposes owing to their inherent medicinal properties, non-toxicity, and diverse functionalities. Aloe vera (AV) hydrogel is one of the hydrogels that have been immensely utilized by humans for centuries due to their numerous therapeutic effects such as wound healing, anti-inflammatory, anti-bacterial, anti-aging, and antiseptic properties.[47],[48],[49] AV hydrogel contains almost 95% water along with 75 potentially bioactive compounds including lipids, amino acids, enzymes, polysaccharides, vitamins, and minerals[50]. For example, AV gel contains polysaccharides, notably acemannan, which possess a remarkable ability to bind to cell membranes and plasma proteins. This characteristic facilitates the acceleration of wound healing by augmenting the production of

collagen.[51] Furthermore, polysaccharides stimulate fibroblasts to produce vital components for extracellular matrix restoration, namely hyaluronic acid and hydroxyproline.[52]. Also, barbaloin and other polyphenolic compounds act as antioxidants to inhibit free radicals mediated cytotoxicity and lipid peroxidation to provide firmness and hydration to the skin[53]. Despite having diverse and countless medicinal perks, the poor mechanical strength of AV gel constrains its utilization in biomedical applications. Different strategies have been reported to increase the mechanical strength of AV hydrogel by reinforcement of stiffer material such as alginate[54], chitosan[55], cellulose[56], gelatine[55], collagen[57] with tuneable mechanical strength. Seppala et.al. reported reinforcement of cellulose nanofibers in AV gel to develop 3D geometries via the direct ink writing method.[58]

Nevertheless, globular proteins have a propensity to self-assemble into amyloid fibrils, which are implicated in number of neurodegenerative diseases in vivo[59]. These amyloid fibrils are widely recognized as the stiffest biological material with mechanical strength comparable to steel.[60],[61] Amyloid fibrils are a good candidate for nanobiotechnological applications because they tend to form hydrogel with excellent stability and tuneable mechanical characteristics under specific physicochemical condition.[62] This amyloid-based hydrogel possesses remarkable biocompatibility and controlled biodegradability owing to the highly ordered structure and multifunctional moieties of the protein molecule. Recently, researchers have demonstrated in vitro amyloid fibrils-based hydrogel formation using diverse proteins such as Bovine Serum Albumin (BSA)[63], lysozyme[64], lactoglobulin[65], etc. In particular, BSA acquired lot of attention due to low cost and biocompatibility. It is a 66 kDa protein derived from cow serum that comprises a single polypeptide chain of 583 amino acids and has 17 cysteine residues.[66],[67] Additionally, cysteine residues of BSA use self-

assembled disulfide linkage to form cross-linked stable hydrogel under certain conditions, such as a change in pH, temperature, or the addition of cross-linking agent.

Herein, a novel and composite hydrogel has been developed by integrating AV in BSA at varying concentrations near and above the melting temperature of BSA. To the best of our knowledge, this is the first instance of creating a printable hydrogel which incorporate AV gel in amyloid-based protein BSA. The proposed hydrogel was thoroughly investigated to determine its physical and chemical properties, revealing its highly porous structure, excellent UV absorption, bright fluorescence, and adjustable rheological properties. As shown in scheme 1, both in vitro and in vivo testing of the composite hydrogel revealed accelerated chronic wound healing efficacy. Further, we developed stable 3D printed geometry with high shape fidelity for tailored wound dressing applications.

3.2 RESULTS AND DISCUSSION

Composite BSA+AV hydrogel was obtained by heating precursor solutions above the melting temperature of BSA 70 ^{o}C. The solution was heated until it formed a translucent gel that passed the vial inversion test in the shortest possible time[68]. The prepared hydrogels were prepared at fix concentration of 80 mg/ml with varying concentration of AV. They are labelled as: AxB8, where x= 8, 6, 4, 2, and 0 %w/v of AV gel powder in fixed concentration of BSA solution (80 mg/ml). All the preheated solutions showed high negative zeta potential as depicted in figure 3.1A. The value of zeta potential indicates high surface charges presence on the surface of the protein leading to excellent dispersion stability and preventing aggregation of BSA due to electrostatic repulsion. The gel formation is confirmed by the vial inversion test as depicted in figure 3.1B Initially, the solution is in liquid form, then transform

into a jiggly gel, and finally turns into a soft gel. These hydrogels were lyophilized at -80°C for 24 h and stored at 4°C for further analysis. Synthesized hydrogels were characterized to investigate various physical and chemical properties. It is observed that gelation time

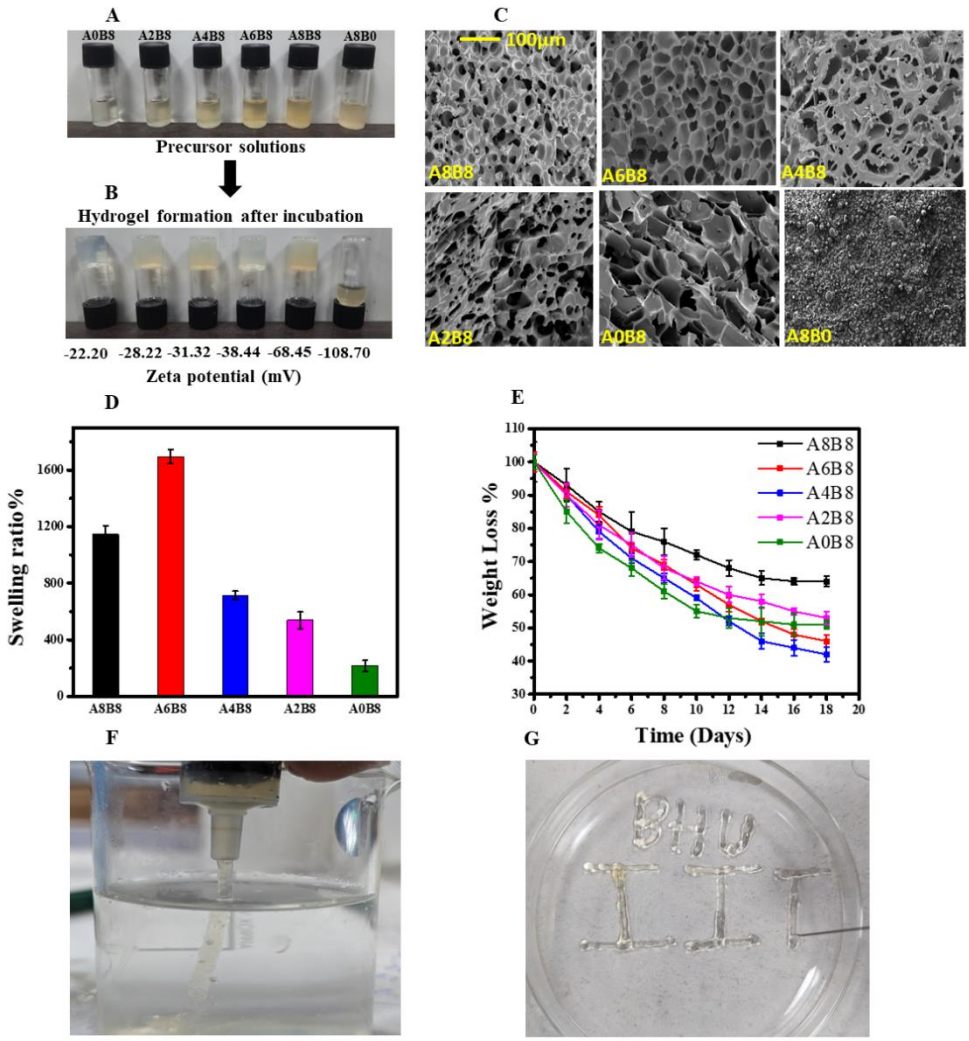

Figure 2.1 The vial inversion test and microscopic images of hydrogels. (A) Preheated precursor solutions with zeta potential value. (B) An illustration of a vial inversion test for various compositions of BSA and AV hydrogel. (C) SEM images of hydrogels representing highly porous structure. (D) Swelling ratio of hydrogels after 24 hr. (E) Weight loss study of hydrogels. (F, G) Injectable behavior of A6B8 hydrogel in water through syringe.

increased with the increased concentration of AV gel. With increase in the concentration of AV gel, which in turn can decrease intermolecular interaction between BSA molecules resulting in slower hydrogel formation. BSA is well known to form concentration-dependent gelation when heated near and above melting temperatures at pH away from its isoelectric point[69]. This phenomenon is initiated by the partial unfolding of BSA resulting in the weakening of hydrogen bonds within the monomer due to thermal fluctuations and hence exposing hydrophobic residues resulting in an aggregation process by an interaction balance between hydrophobic and electrostatic interactions.[70],[71],[72].

Table 2.2 Representing average area (µm2), standard deviation (µm2), and average length (µm) of hydrogel porosity.

Sample	**Average Area (μm^2)**	**Standard deviation (μm^2)**	**Average length (µm)**
A8B8	25.97	3.65	55
A6B8	29.23	2.66	60.43
A4B8	24.66	13.39	53.66
A2B8	16.12	12.22	34.32
A0B8	39.33	14.86	84.04

3.2.1 Morphology and Porosity

Surface morphology and porosity of hydrogels were observed by SEM images of lyophilized samples, depicted in figure 3.2B. All composite hydrogels exhibit highly porous structures with micron-sized voids. Interestingly, as shown in table 1, when the concentration of AV gel is increased, the composite hydrogels exhibited a uniform honeycomb-like three-dimensional supramolecular assembly due to their ability to form hydrogen bond networks with BSA. It is observed from the SEM image that A8B8 shows an overexpression of AV, leading to a reduced degree of porosity in its morphology. Consequently, it is postulated that A6B8 represents a more advantageous candidate, with its optimized and well-organized porosity standing out as a notable attribute. The pore size and interconnectivity of a hydrogel can be adjusted through the modification of its AV content. This enables the synthesis of porous hydrogels with tunable structures. Moreover, it is hypothesized that since the BSA is heated slightly below its melting temperature, secondary structure, or beta sheets formation is still present. Consequently, weaker and less intermolecular physical bonds form between partially denatured BSA molecules, which induces resolubilization of the gel when it is cooled to room temperature[68]. The exact gelation temperature of composite hydrogels was determined by rheometer temperature sweep, figure 3.2A.

The swelling of the lyophilized hydrogel was examined to investigate the capability of hydrogel dehydration for transportation/storage and prior-to-use rehydration as a wound dressing. It is observed that composite hydrogels showed a relatively high swelling ratio with a gradual increase with the concentration of AV gel monitored after 24 h, table 3. 2. Controlled A0B8 hydrogel revealed a degree of swelling of 210 % after 24 h. As expected, composite hydrogels swelling ratio reached as high as 1750 % when AV gel is maximum (A8B8). The

high swelling ratio for composite hydrogels is attributed to the hydrophilic compounds present in AV and BSA, which effectively absorbed water molecules. It can be further hypothesized that the high swelling ratio of composite hydrogels is due to uniform and interconnected voids which provide adequate free volume to accumulate the water entering the hydrogels. Thus, this pattern of swelling ratio is in good agreement with SEM images and rheological observations. The weight loss study of hydrogels is crucial for the wound healing process. If the hydrogel degrades too quickly, it may not provide adequate support to the wound and may impede the healing process. Conversely, if the hydrogel degrades too slowly, it may prolong the healing time, leading to complications such as infection. Therefore, understanding the weight loss behaviour of hydrogels is essential in developing effective wound healing materials. Figure 3.1E described the weight loss of all hydrogels examined over a period of 15 days. All hydrogels showed negligible weight loss due to a well cross-linked polymer network. However, hydrogels with higher BSA content exhibited significant weight loss attributable to a double cross-linked network of protein including hydrogen bonds, beta-sheet crystalline domain, hydrophobic groups, and high crystalline structure, which undergoes rapid degradation. In addition, there would be significant cleavage between hydrogen bonds and hydrophobic bonds, which causes decomposition of the hydrogel network. The injection process of A6B8 hydrogel is illustrated in Figure 3.1 (F, G), showing that it can be extruded smoothly from a 19 G needle with an inner diameter of 0.5 mm without any blockage. This hydrogel ink allows for successful dispensing through a syringe and can be used to fill moulds of varying shapes. In cases of irregular or deep wounds, this hydrogel wound dressing can be conveniently injected into the wound area, adhering well to the wound, and conforming to its shape.

3.2.2 Rheological analysis

Temperature ramp was performed to determine the gelation temperature and phase changes of different solutions. To evaluate this, G' and G" were plotted as a function of temperature at a constant frequency of 10 rad/s and constant strain 1%. Initially, at low temperature (below

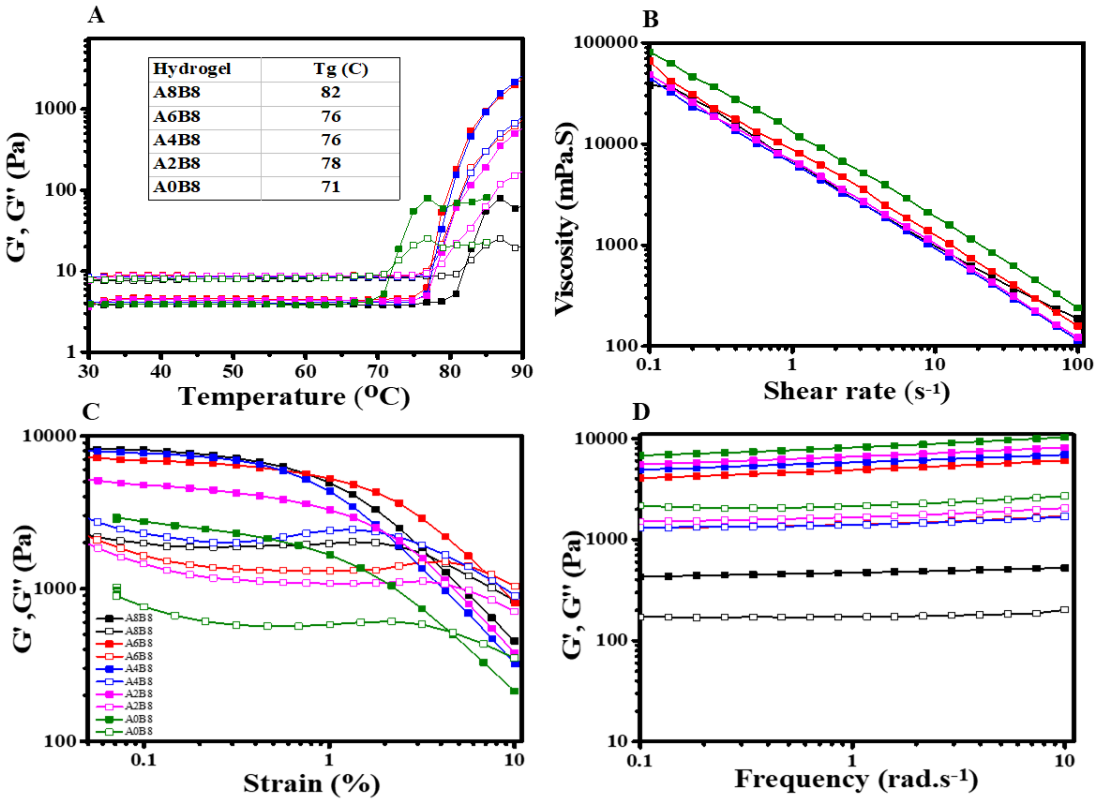

Figure 2.1 Rheological characterizations of hydrogels: (A) Temperature sweep describing gelation temperature at cross point of G' and G". (B) Viscosity curve showing shear thinning behaviour of hydrogels. (C) Amplitude sweep at a constant frequency of 1 rad.s-1 (D) Frequency sweep at a constant shear strain of 1%. Inset in A represents gelation temperature of hydrogels. Green represents A0B8, pink represents A2B8, blue represents A4B8, red represents A6B8 and black represents A8B8. Filled blocks and unfilled blocks represent G' and G" respectively.

70^{o}C), loss modulus was dominant due to low viscosity. With further increase in temperature, there is a sharp increase in storage modulus due to formation of gel at that temperature. As observed, the gelation temperature was found in between 70^{o}C to 80^{o}C for all the different composition hydrogels. From figure 3.2 A it is seen that the gelation temperature increased with AV concentration, indicating late-onset gelation, which is further supported by the vial inversion test, figure 3.1A.

The rheological properties of hydrogels play a vital role in 3D extrusion to fabricate the required structure. For extrusion-based 3D printing, hydrogels must possess shear thinning behaviour. This behaviour is characterized by a change in viscosity as the shear rate increases. As shown in figure 3.2 B, smooth curves revealed that hydrogels show excellent shear thinning nature indicating formation of uniformly cross-linked hydrogel[73].Under shear, superstructures have been broken down into their aggregates and resulted in formation of immobilized hydrogel network, free to move with increasing shear rate.[73],[74] Interestingly, all hydrogels show similar shear thinning behaviour when the shear rate decreases from 100 s^{-1} to 1 s^{-1}.

The viscoelastic properties are further evaluated by performing amplitude and frequency sweep test. Amplitude sweep was performed to determine yield stress and deformation behaviour or linear viscoelastic range (LVR) in the non-destructive deformation range at a constant frequency 1 rad. S^{-1} as described in figure 3.2C. In LVR, storage modulus G' and loss modulus G'' are independent of applied shear strain and hence the curve of G' is used to determine the limiting value or linearity limit of LVR in terms of strain as a percentage[75]. The limiting value was determined at the point where the G' suddenly decreased. For A0B8, G' changed significantly at 1% strain, a linearity limit of strain. While this plateau region

increased with the addition of AV gel due to the formation of a consistent, three-dimensional cross-linked network. Further, all hydrogels revealed a gradual decrease in moduli or breakdown with an increase in strain. This explains the injectable and smooth texture of hydrogels. Also, all hydrogels revealed predominant elastic behaviour at the low shear rate (G'>G") then dynamic yield stress (G'=G'') and viscous nature (G''>G') at the higher shear rate.

In addition, a frequency sweep in the LVR region was also performed to describe the structure and viscoelastic nature of hydrogel as depicted in figure 3.2D. For frequency sweep, a constant strain of 1% is applied and G' and G'' were plotted as a function of frequency. As can be seen from figure 2D, all gels have G' > G'' at given frequency range indicating predominant elastic nature and long-term storage stability due to a stable network of forces[76]. Additionally, both G' and G" are nearly constant and independent across the entire frequency range from 0.1 rad/s to 10 rad/s.

3.2.3 Chemical and Thermal Characterization

The gelation mechanism has been investigated by using UV-Vis spectroscopy. It is well reported that the UV-Vis spectrum of a BSA solution (unheated) shows a typical characteristic

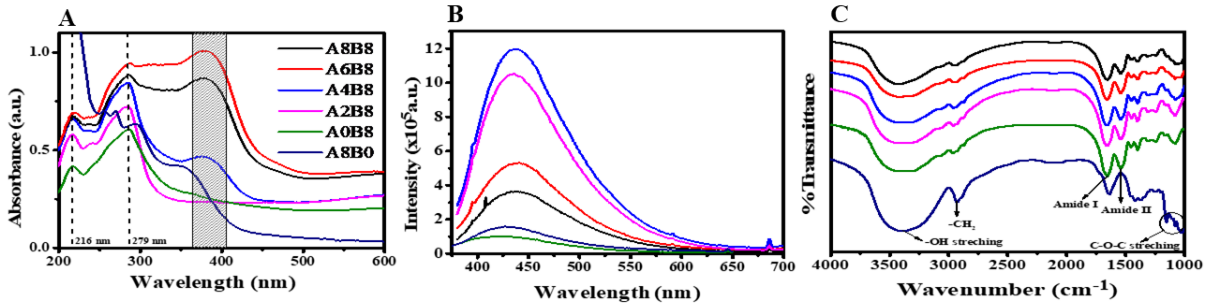

Figure 3.3 Optical characterization of lyophilized hydrogels (A) UV-vis absorbance spectra, (B) Photoluminescence spectra, and (C) FTIR spectra confirming the presence of protein

peak at 279 nm caused by aromatic amino acids tyrosine, tryptophan, and phenylaniline.[77] When the BSA solution is heated near melting temperature, it begins to aggregate, and eventually forms a gel. Pure BSA hydrogel (A0B8) shows the characteristic BSA peak in addition to another peak at 216 nm, figure 3. 4A. Broad absorption around 279 nm suggests that hydrophobic tyrosine residue gets more exposed while tryptophan residue gets covered more due to the hydrophobic microenvironment in the formation of the gel[68]. On the other hand, pure AV gel shows multiple absorption peaks at 352 nm (UV A region), 294 nm (UV B region), and 269 nm (UV C region), as shown in figure 3A. The presence of carbonyl groups and phenolic compounds in AV accounts for the wide absorption peak observed at 352 nm.[78] It is well reported that typical UV absorption observed in Phyto-extract arises due to the existence of conjugated double bonds presented in phenolic compounds of Phyto-origin[52]. Interestingly, composite hydrogel of AV+BSA, particularly A8B8 and A6B8, exhibited wide absorption over the entire UV range, suggesting the possibility of generation of multiple new fluorescent moieties on the surface during the gelation process.

The photoluminescence of composite hydrogels was studied and compared with pure AV hydrogel and controlled BSA hydrogel. Figure 3.3B depicts the fluorescence spectra with an excitation wavelength of 360 nm. All the hydrogels exhibited blue broad autofluorescence. The origin of bright and wide range fluorescence is still unknown however certain assumptions have been proposed such as quantum confinement effect, surface state, and molecule state.[79],[80] The bright fluorescence observed for pure AV gel can be attributed to the presence of numerous oxygen-containing functional groups and various aromatic compounds. On the other hand, controlled A0B8 hydrogel revealed fluorescence with broad emission between 400 nm to 550 nm. This is assigned to reduction in the steric hindrance of

peptide chains and excessive exposure to the aromatic amino acids such as Tyr, Trp, and Phe which might induce energy transfer among C=C and C=O bonds present in BSA.[77] In addition, broad emission suggests that new fluorophores are formed during the thermally induced gelation process. In composite hydrogels, self-quenching fluorescence was observed at higher concentrations of AV. The exact mechanism of this phenomenon is still debated, however processes such as electron transfer, energy transfer, and formation of new complex compounds might be responsible for self-quenching fluorescence.[81],[82],[83]

FTIR spectroscopy has been performed to identify the chemical bonding and functional groups present in hydrogels of different compositions. All the samples (BSA, AV, and composite hydrogels) show a broad and intense peak at 3500 cm^{-1} mainly due to OH stretching modes of vibration as depicted in figure 3.3C. Since the N-H stretching of amino acids superimposes on the OH stretching vibration bands, a thorough analysis cannot be performed in this region. Pure AV (A8B0) exhibited several distinct spectral features. These include a sharp peak at 2920 cm^{-1}, which corresponds to aliphatic stretching of -CH_2. Additionally, a broad peak at 1470 cm^{-1}-1350 cm^{-1} was observed, which was assigned to non-symmetric -CH_2 scissoring and bending. Another notable feature was a sharp peak at 1650 cm^{-1}, which was attributed to C-O stretching. The presence of polysaccharide sugars, such as mannose and glucose, was also indicated by a spectrum observed at around 1260 cm^{-1} to 1000 cm^{-1}, which corresponded to C-O-C glycosidic symmetric stretching vibrations of acetylated polysaccharides indicating the presence of polysaccharides sugars, such as mannose and glucose.[51] These results are consistent with number of previously reported studies[84]. On the other hand, FTIR spectral analysis of A0B8 (pure BSA) revealed the presence of fingerprint amide band region at 1520 cm^{-1} and 1650 cm^{-1} confirming inherent backbone chain

of the protein is intact throughout the gelation process. In case of composite hydrogels, all the characteristic peaks of A0B8 were also present.[85] Notably, the peaks due to C-O stretching (1650 cm^{-1}) and CH_2 stretching (2920 cm^{-1}) get reduced in the composite hydrogel. It might possible that the interaction between AV gel and BSA occurs by the formation of H bonds. Also, the -OH group, $-NH_2$ group, and -C=O in AV gel may form hydrogen bonds with the -OH group and $-NH_2$ group of BSA. Moreover, polyanionic-polycationic complex could be formed through the creation of ionic interactions between the positively charged molecules of AV and negatively charged residues of BSA. However, based on FTIR results, it is not possible to comment on the formation of a new complexes between AV and BSA due to their similar functional groups.

The thermal degradation behaviour and the stability of hydrogels were analysed using thermogravimetric Analysis (TGA), as shown in figure 3.4A. The pure AV gel and composite hydrogels show degradation and weight loss at different temperatures indicating some chemical changes in composite hydrogels after being heated. For instance, pure AV gel shows first weight loss at a temperature range from 80 ^oC to 150 ^oC due to dehydration of physically absorbed H-bond linked to water. The second mass loss was due to thermal polymer degradation starting at about 210 ^oC. The final weight loss occurred between 400 °C to 700 ^{o} C because of the carbonization of the material. On the other hand, composite and pure BSA hydrogel behave the same way, with a significant shift in second weight loss temperature (250 ^oC) due to protein degradation at high temperature. This suggests that the hydrophilic properties improved with better thermal stability.

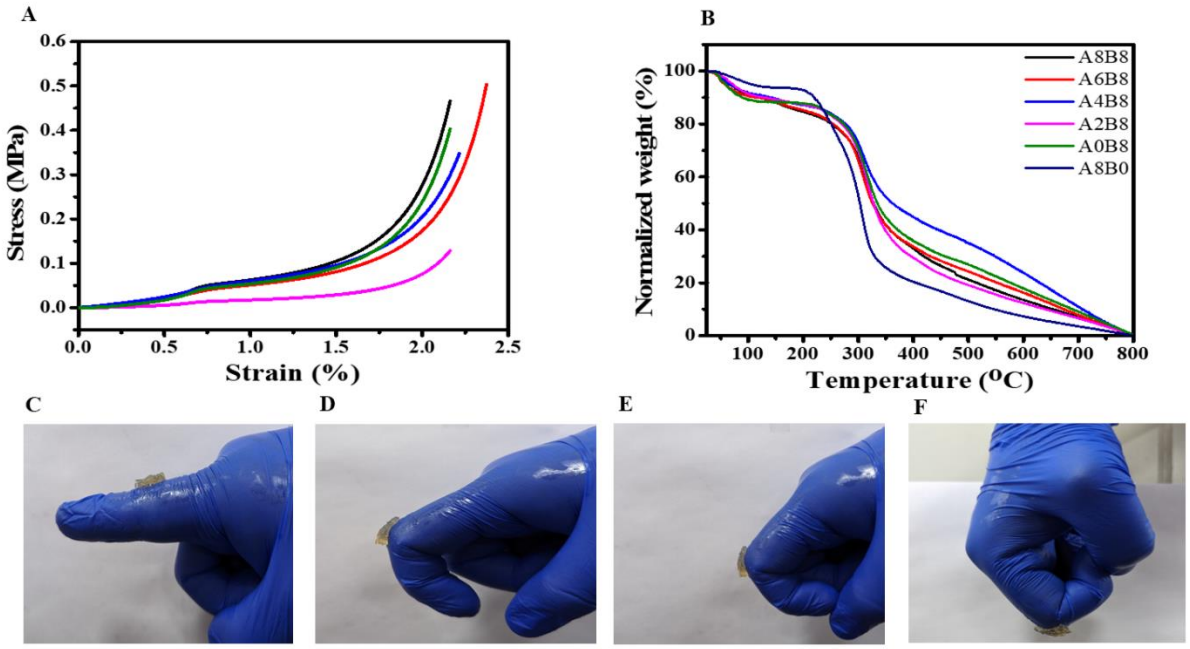

Figure 3.4 (A) TGA thermograms of lyophilized hydrogels. (B) Compression stress-strain curves of hydrogels. (C, F) Images of A6B8 applied on finger joint at different angles.

3.2.4 Mechanical strength

Mechanical properties such as stability and elasticity are required for wound dressing hydrogels and were evaluated using a compression test. As shown in figure 3.4B, all composite hydrogels exhibited excellent stability and maintained structural integrity during compression test. In addition, all composite hydrogels revealed soft and stretchable behaviour, indicating a high degree of crosslinking due to large amount of water trapped in hydrogel pores. The compression modulus increased abruptly after the addition of AV, suggesting the formation of robust and strong matrix owing to the formation of large number of hydrogen bonds with AV. In summary, composite hydrogels demonstrated compatible compression modulus to match requirements and were consistent with what has been reported for wound

healing and tissue engineering applications[81],[86],[58]. Furthermore, it was observed that the hydrogel adhered firmly to the fingers, maintaining its position even when the fingers were bent at angles ranging from 0 to 90 degrees as depicted in Figure 3.4 (C, F). This strong adhesion can be attributed to the robust hydrogen bonding that occurs between the hydrogel and the fingers.

3.2.5 Fabrication and study of 3 D printed scaffold

The optimal outcomes from 3D printing of hydrogels requires careful attention to two key factors: shape fidelity and integrity. Figure 3.5A shows that the mesh structure was successfully printed with A6B8 hydrogel, demonstrating the material's potential for producing high shape fidelity. One of the key advantages of A6B8 hydrogel is its excellent porous

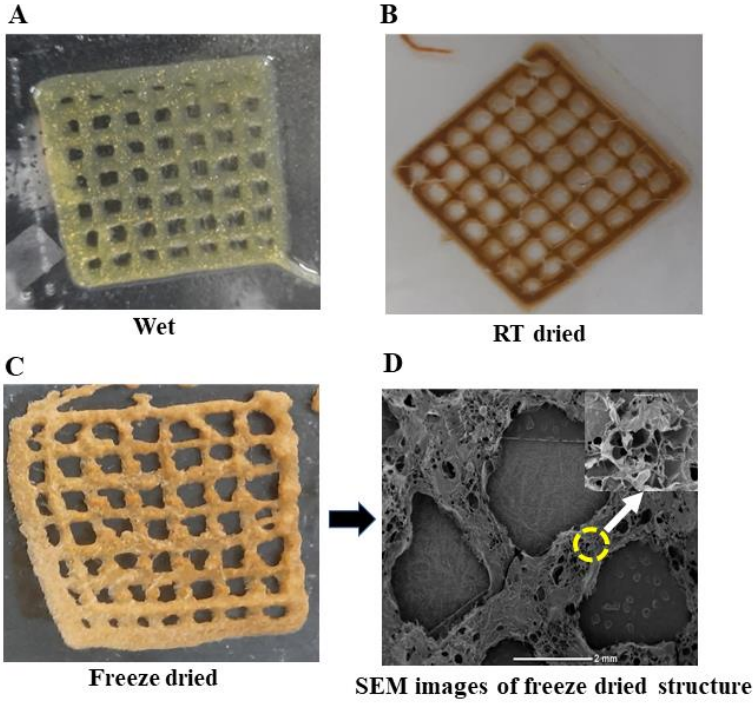

Figure 3.5 3D printed structure of A6B8 hydrogels (A) Freshly constructed wet sample (B) lyophilized sample. (C) Room temperature dried sample. (D) SEM images of 3D printed lyophilized hydrogel structure

morphology and high swelling ratio. This implies that the material flows more easily under the printing conditions, and thickens back after its extrusion from the nozzle. In addition, A6B8 hydrogel has a lower yield stress than the applied stress on the nozzle tip. This means that it is less likely to clog the nozzle or spread out excessively during printing. These properties enable the hydrogel to be printed with good accuracy and fair resolution using a 22

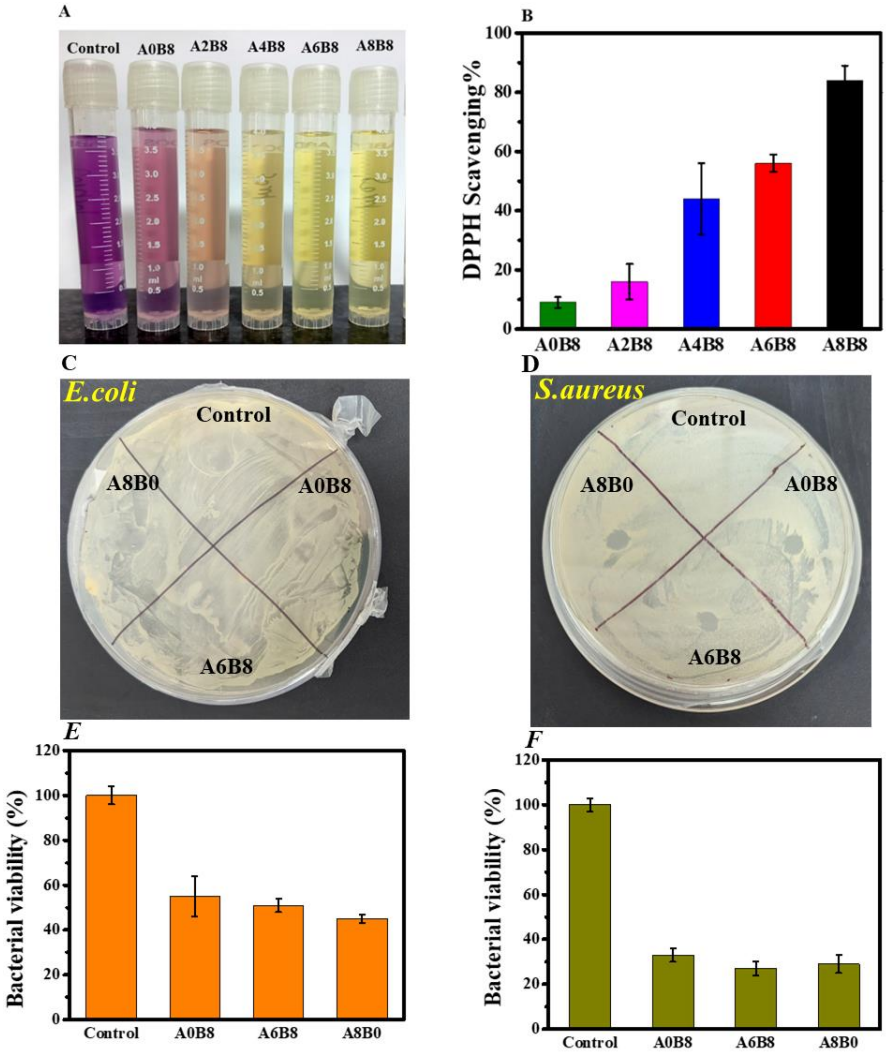

Figure 3.6 (A) Absorbance change of DPPH when exposed to hydrogels (B) DPPH scavenging activity with hydrogels. (C, D) Photos of hydrogels antibacterial activity against E. Coli (C) and S. aureus (D). (E, F) % bacterial viability when exposed to hydrogel

G needle. Another important consideration for 3D printing of hydrogels is the possibility of distortion or collapse during or after printing process. However, each layer of the printed structure with A6B8 hydrogel remained intact and self-supporting throughout the printing process, with no sign of collapse or distortion. This is due to the material's exceptional self-supporting properties.

Figure 3.5[B,C] show that the printed structures can be dried in two ways: freeze-drying and room temperature drying. The freeze-dried samples maintained their shape more effectively and uniformly compared to the room temperature dried samples, which exhibited small cracks likely due to trapped water content. This suggests that freeze-drying is a more effective way to preserve the shape fidelity and integrity of the printed structures. .

The SEM image presented in Figure 3.5D illustrated the excellent structural integrity and high porosity of the freeze-dried A6B8 hydrogel samples. This porous nature is a highly desirable trait for certain applications, such as tissue engineering and drug delivery, as it enables the exchange of nutrients and other substances between the hydrogel and its surroundings. These findings demonstrate the potential of A6B8 hydrogel for successful 3D printing, with good shape fidelity and integrity. Furthermore, the unique properties of the hydrogel, such as its self-supporting and shear-thinning behaviour, make it a promising candidate for a wide range of 3D printing applications, including those in the biomedical and industrial sectors.

3.2.6 Antioxidant and antibacterial properties

Antioxidants have been shown to provide numerous health benefits by preventing oxidative stress, which can impede the repair and regeneration of tissue[87]. In diabetes-related diseases, hyperglycemia exacerbates oxidative stress by damaging enzymes and cellular

machinery, as well as increasing insulin resistance. Thus, a composite hydrogel with ROS-scavenging activities may be useful in treating diabetes. The composite BSA+AV hydrogel is a promising option for this purpose, as AV's antioxidant properties have been well-studied, and its excellent radical-scavenging effect is attributed to its ortho hydroxyl groups, which not only provide antioxidant properties by forming intramolecular hydrogen bonding but also stabilize the formed antioxidant radical[88].

The present study examined the antioxidant activities of composite hydrogels by assessing their ability to scavenge free radicals (2,2-diphenyl-1-picrylhydrazyl (DPPH), hydroxyl (OH•)), and total reducing power. DPPH is a free radical that reacts with antioxidants as a hydrogen receptor, and the decolorization of the DPPH radical solution from purple (strong absorption at 517 nm) to colorless was used to measure the antioxidant activities of hydrogels in the DPPH assay. As the concentration of AV increased, the composite hydrogel showed a more significant DPPH scavenging effect than A0B8 (Figure 3.6A). However, we observed that the DPPH scavenging effect of hydrogels decreased with an increase in H_2O_2 concentration, likely due to the higher H_2O_2 concentration that reduced the pore size of the hydrogel matrices, thereby decreasing the diffusion rate of DPPH into hydrogels. For example, A8B8 hydrogel exhibited a DPPH scavenging effect of approximately 92%, while the scavenging effect of A6B8 and A4B8 hydrogels decreased to approximately 60% and 50%, respectively (Figure 3.6B).

Moving on to the antibacterial properties of the composite hydrogel, an ideal wound dressing should possess antibacterial properties to safeguard the wound against external bacteria, restrain the spread of microorganisms at the wound site, and mitigate inflammation. In this research, we employed S. aureus and E. coli to assess the surface antibacterial potential of

hydrogels (as depicted in Figure 3.6C). After a 24-hour incubation at 37°C, composite hydrogels killed more than 50% of S. aureus and E. coli cells, indicating their effectiveness in inhibiting bacterial propagation. However, A8B8 hydrogels caused cell death in over 65% of cells, while A6B8 and A4B8 hydrogels only killed 52% and 50% of cells, respectively as indicated in figure 3.6(D, E). The inhibition zone reflects a reduction in the bacterial colony population in that region. Consequently, we conclude that all composite hydrogels (BSA+AV) possess antibacterial activity.

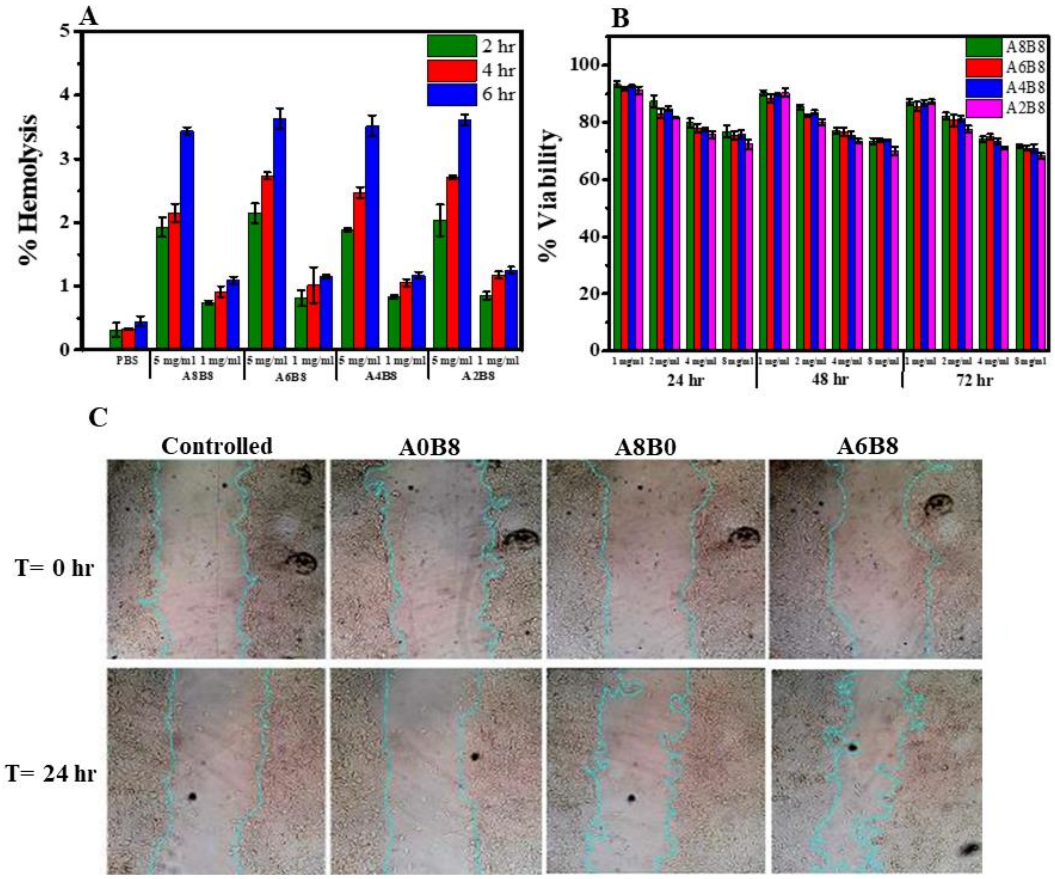

Figure 3.7. In vitro characterization of hydrogels: (A) % viability on NIH-3T3 cell line after 24 hr, 48 hr and 72 hr. (B) Ex-vivo Hemolysis of hydrogels with RBCs after 2 hr (Green), 4 hr (Red) and 6 hr (Blue). (C) Time lapse (0 and 24 hours) images of wound healing closure in NIH-3T3 cells exposed to hydrogels.

3.2.7 In vitro biocompatibility and wound healing assay

Biocompatibility is a necessary step in the development of any compound intended for biomedical applications. In this study, the biocompatibility of hydrogels was evaluated using the MTT colorimetric assay to assess the percentage of cell viability. This assay involves the conversion of MTT to purple-colored formazan crystals by mitochondrial dehydrogenase in live cells. NIH-3T3 cells were cultured in the presence of increasing concentrations of hydrogels (1-8 mg/ml) for 24 h, 48 h, and 72 h, and the cell viability was measured. A dose- and time-dependent decrease in cell viability was observed for A8B8, A6B8, A4B8, and A2B8 hydrogels. This decrease was more pronounced at a concentration of 8 mg/ml, where a decrease of approximately 25-30% occurred after 72 hr. However, the results showed that none of the concentrations used in the study were toxic to NIH-3T3 fibroblast cells, and even at the highest concentration of 8mg/ml, the cell viability was approximately 72-76% after 24 hr. The slight differences in cell viability at each time point were attributed to the concentration of the agent used during their synthesis. The results of this study as shown in figure 3.7A suggest that the prepared hydrogels did not interfere with the mitochondrial metabolism of fibroblast cells and could be a promising material for biomedical applications, such as drug delivery and wound healing. To further evaluate the biocompatibility of the hydrogels, a hemolysis assay was conducted. This assay is considered a simple and reliable method for assessing the biocompatibility of materials. The results showed (figure 6B) that the hydrogels with concentrations of 1 mg/ml and 5 mg/ml exhibited very low hemolytic activity compared to the positive control after 2 h, 4 h, and 8 h. The hemolytic performance of the hydrogels was verified with the positive control Triton X–100 and the negative control phosphate buffer saline (PBS). The interaction of the hydrogels with red blood cells (RBCs)

showed a hemolysis percentage of less than 5%, the critical safe hemolytic ratio for biomaterials according to ISO/TR 7406, indicating that the damage of the hydrogels on the RBCs was minimal even after 8 h of incubation time at both concentrations used during the study. In conclusion, the results of this study indicate that the investigated hydrogels are biocompatible and can be a potential candidate for biomedical applications. The MTT assay and hemolysis assay showed that the hydrogels did not cause significant toxicity to cells or RBCs, respectively. These findings suggest that further in vivo studies could be conducted to explore the efficacy of these hydrogels in biomedical applications.

In this study, we investigated the effect of hydrogel-containing medium on wound healing using an in vitro cell model. Our findings, as depicted in figure 3.7C, demonstrated that the hydrogel promoted wound healing. We observed a reduction in the scratch area of the wound after 24 hours of exposure to the hydrogel, as compared to the control group. Moreover, the width of the scratch was also decreased after 24 hours in the presence of the hydrogel. The standard deviation of the scratch width was analyzed to understand the heterogeneity of the scratch width at each time point, and it suggested differences in the migration patterns of the cells. Interestingly, the deviation of the width did not appear to be influenced by the evaluation time or the type of medium used. Our results also showed that the rate of cell migration increased after exposure to the hydrogel, and it approached an average value of 4.21 μm/hr after 24 hours until the end of the experiment. These findings suggest that the hydrogel-containing medium may have potential applications in promoting wound healing.

3.2.8 In vivo study

Wound healing is delayed in Diabetes mellitus individuals due to chronic hyperglycaemic condition. The functional wound healing properties of herbal phytochemicals could be a strategic approach for progressive wound healing in diabetes condition[89]. In this context, our study has aimed for better healing through tropical application of hydrogels which are very emergent in comparison to conventional approach. In this in-vivo study performed for chronic wound healing potential of hydrogels prepared from BSA, AV and combination of BSA, and AV was carried out on the chronic diabetic wound model in wistar rat induced by streptozotocin (STZ). The administration of STZ for inducing diabetes mellitus is a widely used method for assessing the healing properties of herbal-based hydrogels[90]. STZ is a diabetogenic agent that naturally occurs as an alkylating antineoplastic agent and is particularly hazardous to the insulin-producing beta cells of the pancreas in mammals. The glucose transporter is responsible for the uptake of STZ by pancreatic β-cells, resulting in cellular damage characterized by DNA fragmentation and apoptosis. Concurrently, the accumulation of reactive oxygen species, such as hydrogen peroxide, is observed, which further exacerbates the deterioration of cellular function. These pathological events culminate in impaired insulin production and glucose homeostasis, manifesting as hyperglycemia. Diabetes diseased model was initially developed when they received dose of STZ ranging from 50 to 65 mg/kg[91],[92],[93]. The concentration of STZ and route of administration determine the formation of induced diabetes mellitus model. For validation of diabetes mellitus model was done, where glucose level was measured, level of glucose above >250mg/dL is induced with diabetic mellitus, further excisional wound was formed for diabetes wound related studies. The mean glucose level for all groups was represented

as mg/dL; however, topical treatment of diabetic rats' wounds with different hydrogel formulations did not result in any significant alteration in their blood glucose levels. (figure 8B). The role of STZ on the body weight of wistar rat was also monitored, which was found to be reduced after intraperitonial administration of STZ. The mean body wt. for all groups was represented in gram; however, the body wt. loss was observed in the diabetic rats irrespective of topical treatment of the wound using different hydrogel formulation post

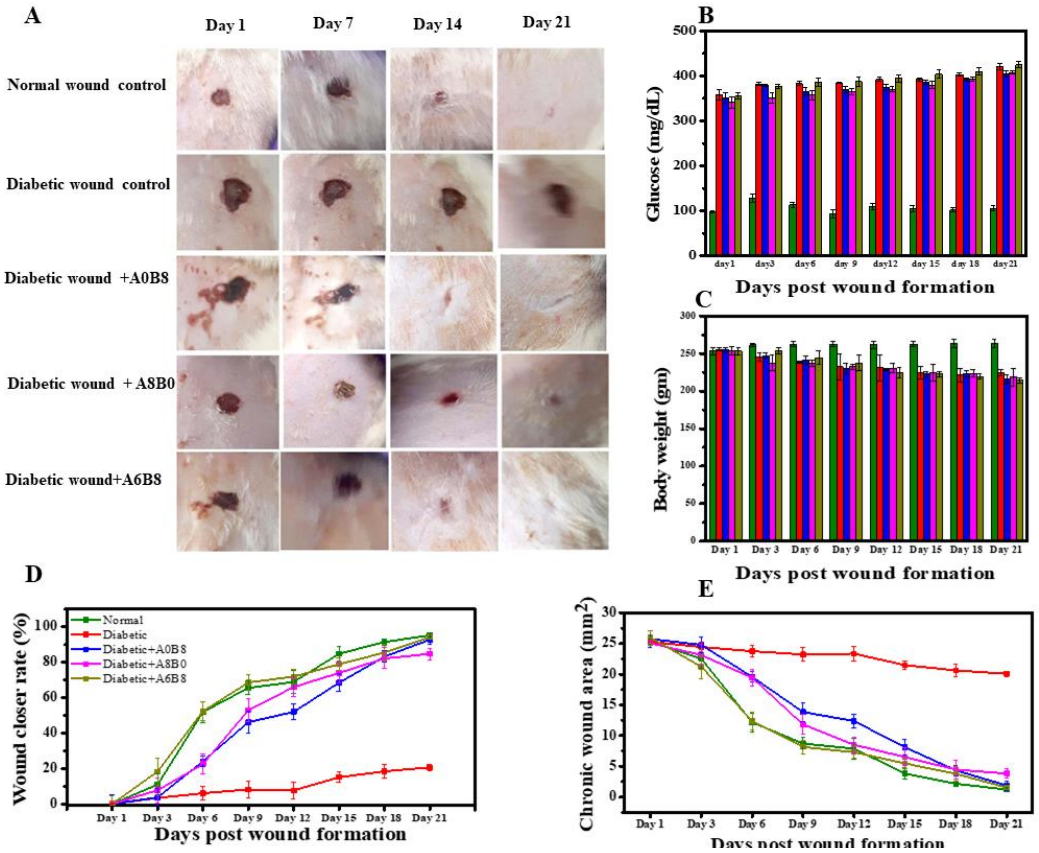

Figure 3.8. (A) Representative photographs for macroscopic assessment of wound healing for 5 groups (normal, diabetic control, diabetic + A0B8, diabetic + A0B8, diabetic+A8B0) and recorded at 1st, 7th, 14th 21th post wound formation. (B) Effect on blood glucose level in control and treated groups post wound formation. (C) Effect on body wt. in control and treated groups post wound formation. (D) Effect of hydrogel treatment on chronic wound healing rate in control and treated groups post wound formation. (E) Effect on chronic wound area in control

wound formation as described in figure 3.8C. Moreover, excessive protein and lipid breakdown and/or dehydration may be linked to the body weight loss, as seen in diabetic rats.[93],[94]

Throughout the experiment, regular macroscopic qualitative analysis was performed. Initially, all wounds exhibited similar appearance on the first day of wound induction; however, significant differences in both wound area and morphology were observed and depicted in figure 3.8A. From days 7 to 21, distinct scar formation from necrotic tissue residue was observed in various groups, along with noticeable clinical signs of inflammation, such as redness and swelling, which were alleviated by the topical application of hydrogel formulation. Furthermore, re-epithelialization was observed, and the A6B8 treated group showed a faster rate of re-epithelialization. Further wound healing was evaluated in terms of chronic wound area and wound closure rate. It reveals that the wounds in the group represented as diabetic wound+ A6B8 treated showed more rapid contraction significant to those in the normal control (1.202±0.299mm^2; 95.241±1.183%) and diabetic control (20.060±0.417 mm^2; 20.645±1.650%) groups, with wound closure area and closure rate of 1.533±0.310mm^2; 94.091±1.197% as shown in figure 3.8(D,E). For diabetic wound+A0B8 treated and diabetic wound A8B0 treated groups the values are 1.852±0.743mm^2; 92.801±2.887% and 3.814±0.804mm^2; 84.778±3.209% respectively. This finding suggests enhanced healing with combination of both BSA and AV together in comparison to diabetic wound control.

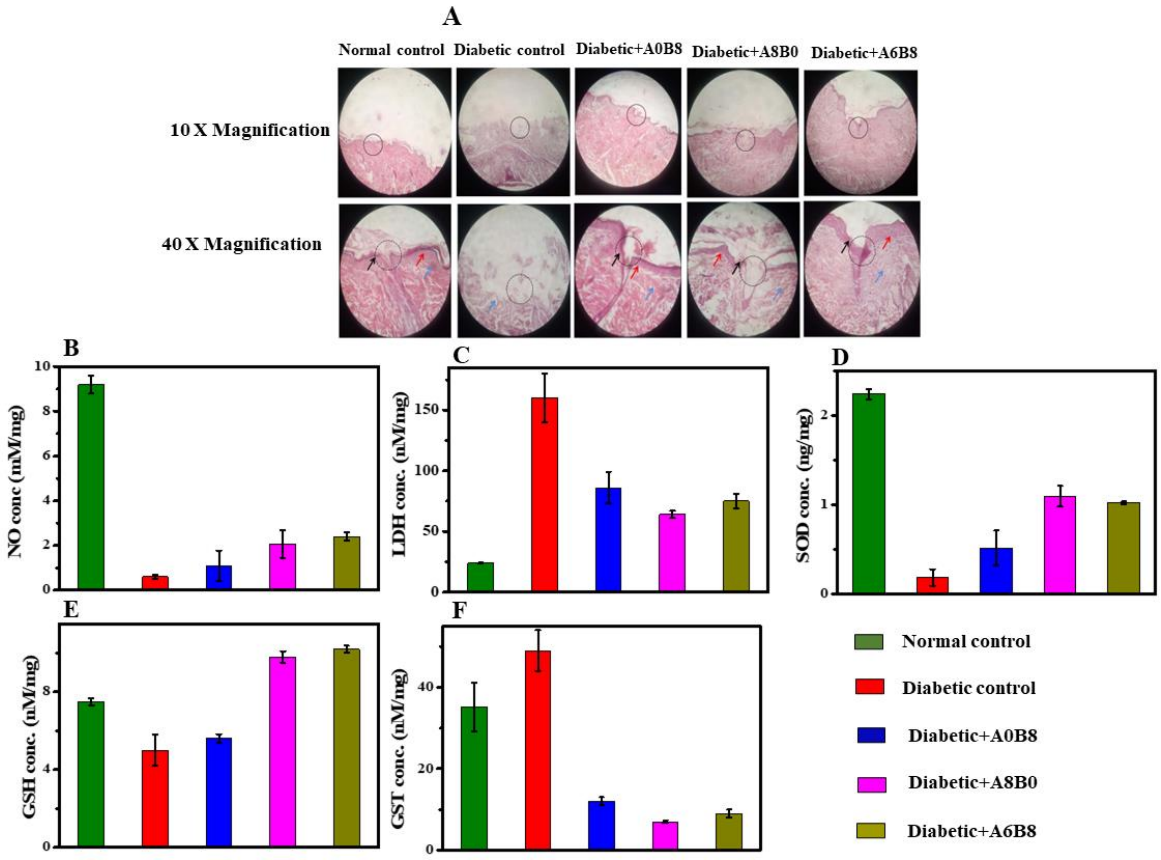

Figure 3.9 (A) Histopathological anatomy of wound tissue: Columns 1-5 represent different groups, row 1-2 represent different magnification at which image is visualized. Black arrow (E): Re-epithelialization; Blue arrow (C): Collagen; Red arrow (Fb): Fibrosis. Region marked in black circle is wound area. (B, F) Effect on NO conc., LDH conc., SOD conc., GST conc., and GSH Conc. after hydrogel treatment in control and treated groups in wound tissue.

Effect of STZ on physiological homeostasis was determined in terms of cellular ROS generated, specifically free radicals of oxygen and nitrogen represented as reactive oxygen and nitrogen species (ROS and RNS) constitute the final healing mechanism, where origin of the oxidative stress has complicated the healing process. STZ administration increases protein glycation, lipolysis, ketogenesis etc. and decreased antioxidants substrates such as glutathione

(GSH), Nicotinamide adenine dinucleotide phosphate dependent coenzyme Q reductase (NaD(P)HCoQ) levels. Further level Nitric oxide (NO) and lactate dehydrogenase (LDH) are biomarkers that indicate oxidative stress in diabetic condition. Special focus on 3 isoenzymes for NO synthase i.e., eNOS, iNOS and nNOS, which promote NO generation via catalysing the oxidation of L-arginine to L-citrulline in a nicotinamide adenine dinucleotide phosphate reduced form (NADPH) and oxygen dependent reaction. Studies indicate role of eNOS is mainly used as a marker for angiogenesis in diabetic wound condition while iNOS was mainly used as an index for NO production. Therefore, both eNOS and iNOS play important role in healing process.[95],[96] It has been reported the that STZ destroys pancreatic beta cell that leads to hyperglycemia-induced altered glucose transport, dysfunctional mitochondrial bioenergetics and imbalance in the rate of oxygen utilization by respiratory chain complexes responsible for non-healing complication. Oxidative stress and effective NO production was measured as values obtained from NO assay (figure 3.9A), for diabetic wound+A0B8 treated group it is 1.085±0.693μM/ mg and diabetic wound +A8B0 treated groups it is 2.061±0.624μM/ mg but for diabetic wound + A6B8 treated it is increased to 2.433±0.177μM/ mg with respect to normal (9.296±0.461μM/ mg) and diabetic control groups (1.085±0.693μM/ mg) (figure 3.9B). For LDH assay as cellular biomarker for compromised cell membrane integrity (figure 3.9C). The values for diabetic wound +A0B8 treated group is 86.127±13.497nM/ mg and diabetic wound +A8B0 treated groups it is 64.403±3.815nM/mg but for diabetic wound + A6B8 treated it is increased to 75.771±6.893nM/ mg with respect to normal (24.805±0.342nM/ mg) and diabetic control groups (160.133±20.578nM/ mg) (figure 3.9C).[97] However, ROS generation in tissues is regulated by inhibition of electron transfer at Complex I (by rotenone) that augments radical formation. Oxidative stress related assays

performed so far represent reduce levels of oxidative stress as it promotes the healing mechanism in wound tissue post wound formation on application of applied hydrogel formulation. Superoxide dismutase is another free radical scavenger enzyme that rapidly catalyzes the dismutation of superoxide anion (O-·) and thus acts as a first line antioxidant defence mechanism. In the case of Superoxide dismutase (SOD) deficiency, superoxide anion reacts with NO to produce peroxynitrite (ONOO-), which is a potent oxidant and nitro sating agent that can cause direct damage to proteins, lipids, and DNA. Under diabetic wound condition concentration of SOD enzyme in the group represented as diabetic wound + A6B8 treated showed 1.023±0.015 ng/ mg of SOD enzyme present in wound tissue, for diabetic wound +A0B8 treated and diabetic wound +A8B0 treated groups the values are 0.517±0.195 ng/mg and 1.098±0.117 ng/mg, further it was also compared to normal control where values were shown to be 2.240±0.058 ng/mg and in diabetic control group it was 0.187±0.094 ng/mg respectively (figure 3.9D)[98]. Concentration of GSH in the group represented as diabetic wound BSA+ AVtreated group showed GSH conc. of 10.199±0.172 nM/mg on comparison to normal control (7.564±0.180nM/mg) and diabetic control (5.008±0.838nM/mg) groups (figure 3.9E). For diabetic wound +A0B8 treated and diabetic wound +A8B0 treated groups the values are 5.635±0.239 nM/ mg and 9.810±0.371 nM/ mg respectively[99] (figure 3.9E). Further the values for GST assay for diabetic wound +A0B8 treated group is 12.909±1.388 nM/ mg and diabetic wound +A8B0 treated groups is 7.532±0.362 nM/ mg but for diabetic wound + A6B8 treated group it is increased to 9.302±1.333 nM/ mg with respect to normal 35.191±6.272nM/mg and diabetic control groups (49.959±5.242 nM/ mg) (figure 3.9F). Thus, when wound repair is defective, stimulating collagen production would be advantageous for potential healing of chronic wound. The findings indicate that the administration of AV in

conjunction with BSA via topical application stimulates collagen deposition and accelerates wound healing. This process is facilitated through heightened expression of vascular endothelial growth factor (VEGF), an endogenous angiogenesis stimulant, and its receptors which are upregulated during wound healing. The upregulation of VEGF and its receptors increases the supply of oxygen and essential nutrients necessary for collagen synthesis at the chronic wound site. This finding suggests enhanced healing with combination of both BSA and AV together in comparison to normal control and the diabetic wounds.

Histopathological examination performed post 21 days after fixation of wound tissue following hematoxylin eosin (H&E) stain. It reveals epithelialization in normal control and diabetic hydrogel treated groups, there was no epithelialization seen in diabetic control as described in figure 3.9A. Further orderly arrangement of collagen content of granulation tissue in diabetic control group is also very low, probable confirming the presence of persistent inflammation and high level of oxidative stress. Fibroblast proliferation under epithelium also covered wound area in normal control. However, there are no inflammatory cells seen. Although process of epithelialization was complete in the A6B8, fibroblast and collagen regeneration were also more evident in the A6B8 with proper arranged in bundles and sited parallel to the newly formed epidermis on comparison to A0B8 and A8B0.[100]

3.3 Conclusion

In this study, we developed a novel composite hydrogel by integrating AV hydrogel in BSA at varying concentrations. To our knowledge, this is the first instance of creating a printable hydrogel based on AV and BSA. We found that the A6B8 sample represents a more advantageous candidate, with its well-organized porosity, high swelling ratio and water

uptake standing out as a notable attribute. We conducted both in vitro and in vivo testing of the composite hydrogel, and the results showed accelerated chronic wound healing efficacy. These results suggest that topical application of A6B8, stimulated the deposition of collagen and thereby promoted the wound healing through increased expression of VEGF, leading to improved angiogenesis and delivery of necessary nutrients for collagen synthesis. This finding suggests enhanced healing with combination of both BSA and AV together in comparison to normal control and the diabetic wounds. Moreover, the 3D printability of hydrogel enables to customize the dressing to individual wounds makes it a promising option for personalized diabetic wound care. Overall, BSA-AV hydrogel has shown to be a promising solution for personalized diabetic wound healing. Its unique combination of properties and the ability to customize the wound dressing to the specific needs of each patient makes it a valuable addition to the current wound healing options. However, further research is needed to evaluate the long-term effectiveness of this wound dressing in a clinical setting.